*Geophys. J. Int.* (2004) **158,** 998–1008 doi: 10.1111/j.1365-246X.2004.02333.x

# Imaging of three-dimensional small-scale heterogeneities in the Hidaka, Japan region: coda spectral analysis

Taka'aki Taira and Kiyoshi Yomogida

*Division of Earth and Planetary Sciences, Graduate School of Science, Hokkaido University, North* 10 *West* 8, *Kita-ku, Sapporo* 060-0810, *Japan.*
*E-mails: taka@noreply.ep.sci.hokudai.ac.jp (TT); yomo@ep.sci.hokudai.ac.jp (KY)*

Accepted 2004 April 13. Received 2004 March 19; in original form 2003 April 23

## SUMMARY

While large-scale heterogeneities have been studied intensively by seismic tomography with traveltime data, small-scale heterogeneities are not fully investigated yet. We obtained the 3-D spatial distribution of small-scale heterogeneities as relative scattering coefficients in the Hidaka, Japan, region using the spatial variation of high-frequency coda power spectra. We analysed 530 seismograms recorded at 62 stations for nine local earthquakes in the frequency range of 1–32 Hz. After correcting source, station and propagation effects, we assigned the spatial and temporal variations of observed power spectra of coda waves into the 3-D distribution of scattering coefficient, based on single and isotropic scattering models. Small-scale heterogeneities are distributed not only in a non-uniform manner but also differently among scale lengths estimated from their frequency dependence. An area of large relative scattering coefficient in 2 and 16 Hz is located at a depth shallower than 45 km in the southwest of the Hidaka Mountains, correlating well with a highly active area of microearthquakes. At a depth of 60–120 km, two dipping zones of large scattering coefficient are imaged beneath the summit of the Hidaka Mountains. These zones may imply two layers of strong seismic-wave reflection, consistent with the upper and lower planes of the double seismic zone in the subducting Pacific Plate, as determined by the hypocentral distribution in this region.

**Key words:** collision belt, lithosphere, scattering, seismic coda.



## 1 INTRODUCTION

Observed seismograms of high-frequency coda waves (>1 Hz) are attributed mainly to small-scale heterogeneities in the Earth (e.g. Aki 1969; Aki & Chouet 1975). The stochastic characteristics of heterogeneities have been studied, using the excitation of incoherent coda wave and the attenuation of high-frequency seismic waves (e.g. Aki 1973; Jin & Aki 1986; Su & Aki 1990). On the other hand, seismic array observation enables us to estimate the spatial distribution of heterogeneities beneath the array in a deterministic manner. Several studies based on such array analysis technique [e.g. semblance analysis and frequency–wavenumber (*f–k*) analysis] quantitatively estimated the distribution of small-scale heterogeneities from coherent arrivals in coda (e.g. Capon 1969; Neidell & Taner 1971; Nikolaev & Troitskiy 1987; Gupta *et al.* 1990). Using the *f–k* analysis, Gupta *et al.* (1990) analysed seismograms at the EKA and NORESS arrays using a nuclear explosion as a seismic source and determined locations of several distinct scatterers. Matsumoto *et al.* (1998) applied the slant stack method to the data of a small-aperture seismic array in the source region of the 1995 Hyogo-ken Nanbu earthquake (M7.2) and showed strong scatterers concentrated just beneath the hypocentre.

Regional dense seismic observations were recently conducted and revealed the distribution of scatterers in a wide area (e.g. Nishigami 1991; Revenaugh 1995; Nishigami 1997, 2000; Revenaugh 2000). For example, Nishigami (2000) used the recursive stochastic inversion to image the 3-D distribution of scatterers around the San Andreas fault. He concluded that the scatterer distribution is related to the geometry of the fault system. Revenaugh (2000) estimated the distribution of scattering potential by the stochastic Kirchhoff migration in southern California. He suggested that the scattering potential is highly correlated with microseismicity level. In order to pinpoint the locations of small-scale heterogeneities, theories and models with realistic scattering processes must be taken further into account.

Another kind of deterministic approach to mapping small scale-heterogeneities is the use of the spectral ratio of coda waves, as used for example by Aki & Ferrazzini (2000), Taira & Yomogida (2003) and Tsuruga *et al.* (2003). These studies showed that coda levels fluctuate significantly and systematically within a dense seismic network. For example, Taira & Yomogida (2003) obtained coda amplification factors in the Hidaka region, including their frequency dependence. A coda amplification factor was defined as the amplitude ratio of coda waves among different stations after correcting

 

for each the site amplification factor that reflects the surface geology (e.g. Quaternary sediment) of each station. They found systematic spatial variations of coda amplification factors, revealing a highly non-uniform distribution of small-scale heterogeneities in this region. As one of their important results, the coda is relatively amplified for paths crossing the Hidaka Mountains in a high-frequency range (>16 Hz). They did not, however, relate the detected coda amplification factors with the spatial distribution of scatterers in the Earth quantitatively.

In this paper, we shall propose a new imaging method, using power spectra of coda waves of high frequency (>1 Hz) as a function of lapse time. We shall also attempt to detect the location of small-scale heterogeneities with large scattering coefficient beneath the Hidaka Mountains, in order to explain the characteristics of coda amplification factors obtained by Taira & Yomogida (2003). Scattering coefficient in this study is defined as the fractional loss of energy of incident seismic wave as a result of scattering by heterogeneities in a medium (Aki & Chouet 1975). We shall discuss the corresponding regional tectonics, such as the subducting Pacific Plate, in the Hidaka collision zone, using frequency dependence in spatial distribution of scattering coefficients.

## 2 MAPPING OF SMALL-SCALE HETEROGENEITIES

As one of the promising recent research movements, the distribution of small-scale heterogeneities has been gradually revealed with the use of dense seismic networks. For example, Matsumoto *et al.* (1998), Nishigami (2000), and Revenaugh (2000) estimated the spatial distribution of heterogeneities in active seismic areas from high-frequency coda waves. Although these studies adopted some sophisticated approaches, all of them were based on the following two fundamental assumptions in the scattering process: single and isotropic scattering models. In this study, we shall also employ theses two assumptions in the relative scattering coefficients. Because the observed seismograms are involved in various complex processes, the following additional assumptions are introduced: scattering in a 3-D half-space with a constant *S*-wave velocity, only *S*-to-*S*–wave conversion and isotropic radiation of *S* waves at each source.

Heterogeneities are expressed as relative scattering coefficient located at each block of the volume $\delta V$ (Fig. 1a). The free surface is treated as a perfect seismic reflector of *S* waves for which the reflection coefficient is one. In order to take this effect into account, scattered waves generated by a mirror image source are introduced in addition to the scattered waves from the original source (Fig. 1b). Because all the hypocentres in this study are relatively deep (>30 km) and located within the model space, the effect of complex velocity structure in this area should be minor. Using the radiative transfer theory, on the one hand, Sato *et al.* (1997) showed that the effect of non-isotropic radiation of seismic waves (i.e. a double couple source) becomes unimportant as the lapse time of coda waves increases, because of the averaging effect of scattered waves. Because we use the coda part of relatively large lapse time (i.e. after the time twice the *S*-wave traveltime) in this study, the assumption of isotropic radiation at each source should not affect the locations and magnitudes of scatterers significantly. In summary, all the additional assumptions in the present analysis should not severely alter our final result of the locations and magnitudes of scatterers.

In contrast with the previous studies that normalized each seismogram by its maximum in the first stage of their data analyses, our present approach tries to map the power spectrum of each coda into scattering coefficients in a medium after the corrections of source, station and overall propagation effects (e.g. the effect of coda $Q$). As for Taira & Yomogida (2003), the relative site amplification factor (*RSAF*) of each station is estimated by the coda-normalization method with regional earthquakes and coda $Q$ is determined by the maximum likelihood method, respectively.

The coda power spectra are then mapped into the relative scattering coefficient at each block by the following three steps.

First of all, we attempt to remove the propagation effect for a given source to each station. The observed amplitude in coda is affected by the energy loss resulting from anelastic or intrinsic attenuation, together with the averaged or background scattering attenuation, along each ray path. We normalize amplitude in coda, using the values of coda $Q$, as obtained in Taira & Yomogida (2003), with the reference starting time of coda wave $t_c$:

$$\overline{v}_{ijk}\left(\tau_{ij}^{\mathrm{obs}}; f\right) = v_{ijk}\left(\tau_{ij}^{\mathrm{obs}}; f\right) \cdot \exp\left[\frac{\pi f\left(\tau_{ij}^{\mathrm{obs}} - t_c\right)}{\widetilde{Q}_c(f;k)}\right], \tag{1}$$

where $v_{ijk}(\tau_{ij}^{\mathrm{obs}}; f)$ indicates the velocity amplitude in coda for the $i$th earthquake at the $j$th station in the $k$th component for the lapse time $\tau_{ij}^{\mathrm{obs}}$ after being passed through a bandpass filter of the centre frequency $f$. $t_c$ is defined as the maximum lapse time of all the data for each earthquake. $\widetilde{Q}_c(f;k)$ is the coda $Q$ averaged over all the seismograms in the $k$th component. $\overline{v}_{ijk}(\tau_{ij}^{\mathrm{obs}}; f)$ may be considered as the normalized velocity amplitude of coda waves because it is already corrected by the overall propagation effect.

Next, we calculate the running power spectrum of $\overline{v}_{ijk}(\tau_{ij}^{\mathrm{obs}}; f)$ with an appropriate time window $\delta t$ (1.28 s in this study) around $\tau_{ij}^{\mathrm{obs}}$, which is expressed by $E_{ijk}(f, \tau_{ij}^{\mathrm{obs}})$. This process smoothes the highly complicated temporal variation of the coda level that

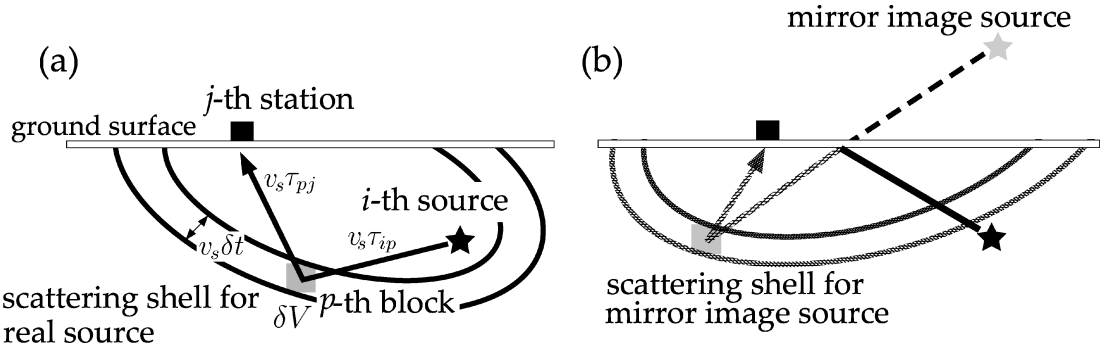


**Figure 1.** Model geometry and scattering ray path of a single scattered wave by the $p$th block of volume $\delta V$ in a homogeneous half-space for the $j$th station with (a) the $i$th real and (b) the mirror image sources. $v_s$ is the share wave velocity and $\delta t$ is the time window.

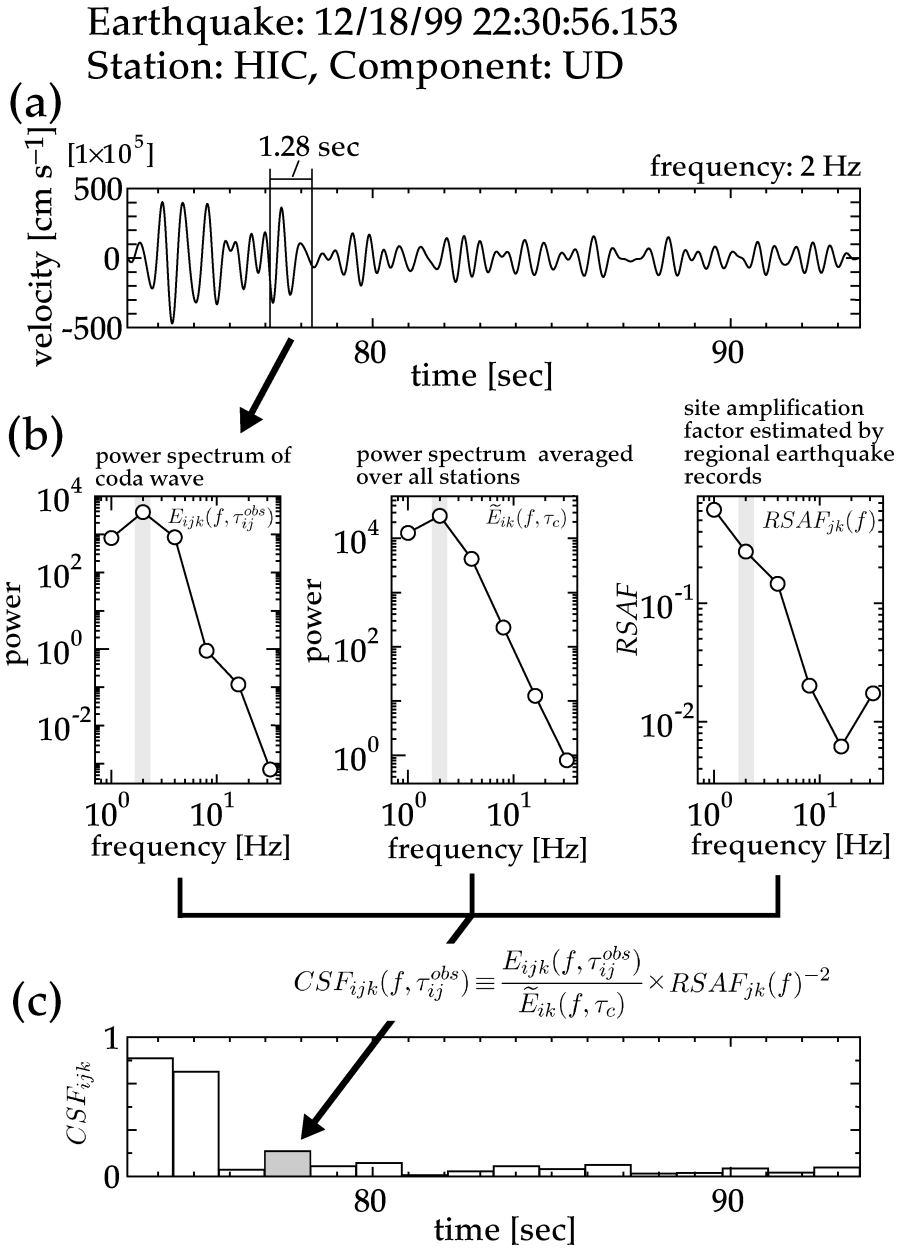


**Figure 2.** Schematic view of the procedure to obtain $CSF_{ijk}(f, \tau_{ij}^{obs})$. (a) Bandpass filtered (with the centre frequency of 2 Hz) seismogram after the correction of coda $Q$. (b) Power spectra of HIC (left) and the average over all the stations (centre) for the earthquake, 1999 December 18. Relative site amplification factor (*RSAF*) of HIC (right) was obtained formerly by Taira & Yomogida (2003). (c) $CSF_{ijk}(f, \tau_{ij}^{obs})$, that is, running power spectra after correction of source, station and propagation effects.

cannot be expressed by the present discretization scale of the model space. The selection of $\delta t$ is based on the relationship of $\delta t < 2(\delta V)^{1/3}/\upsilon_s$, where $\upsilon_s$ is the $S$-wave velocity, so that the isochronal scattering shell at each lapse time $\tau_{ij}^{obs}$ always covers multiple blocks (Fig. 1). Using the single scattering model (e.g. Aki & Chouet 1975; Sato & Fehler 1998), the running power spectrum can be related to the intensity of scattering term $P_{ijk}(f, \tau_{ij}^{obs})$ for the corresponding portion of coda as follows:

$$E_{ijk}\left(f, \tau_{ij}^{obs}\right) = S_{ik}(f)^2 \cdot G_{jk}(f)^2 \cdot P_{ijk}\left(f, \tau_{ij}^{obs}\right) \cdot \exp\left(-\frac{2\pi f \tau_c}{\widetilde{Q}_c(f;k)}\right), \quad (2)$$

where $S_{ik}(f)$ is the source term of the $i$th earthquake, $G_{jk}(f)$ is the station term of the $j$th station and $\tau_c$ is the maximum lapse time for the $i$th earthquake.

Because $G_{jk}(f)$ can be replaced by the relative site amplification factor [$RSAF_{jk}(f)$ for the $j$th station in the $k$th component at frequency $f$], as already obtained from regional earthquakes (Taira & Yomogida 2003), the remaining task is to suppress the source term $S_{ik}(f)$. Analogous to coda duration magnitude (e.g. Sato & Fehler 1998), we define the coda source factor (hereafter called *CSF*) as the ratio of the power spectrum of coda $E_{ijk}(f, \tau_{ij}^{obs})$ to the average over all the stations for a given $i$th earthquake $\widetilde{E}_{ik}(f, \tau_c)$ at the fixed lapse time $\tau_c$, using the corresponding relative site amplification

factor:

$$RSAF_{jk}(f)^{-2} \times \frac{E_{ijk}\left(f, \tau_{ij}^{\rm obs}\right)}{\widetilde{E}_{ik}(f, \tau_c)} = \frac{S_{ik}(f)^2 \cdot P_{ijk}\left(f, \tau_{ij}^{\rm obs}\right) \cdot \exp\left(-\dfrac{2\pi f \tau_c}{\widetilde{Q}_c(f;k)}\right)}{S_{ik}(f)^2 \cdot \widetilde{P}_{ik}(f, \tau_c) \cdot \exp\left(-\dfrac{2\pi f \tau_c}{\widetilde{Q}_c(f;k)}\right)} \simeq \frac{P_{ijk}\left(f, \tau_{ij}^{\rm obs}\right)}{\widetilde{P}_{ik}(f, \tau_c)} \equiv CSF_{ijk}\left(f, \tau_{ij}^{\rm obs}\right). \quad (3)$$

Fig. 2 shows a schematic view of the procedure to obtain *CSF*. Note that the above procedure is presented for each component, then we shall use the sum of the three components of *CSF*:

$$CSF_{ij}\left(f, \tau_{ij}^{\rm obs}\right) \equiv \sum_{k=1}^{3} CSF_{ijk}\left(f, \tau_{ij}^{\rm obs}\right). \quad (4)$$

Finally, we estimate the spatial distribution of relative scattering coefficient. Coda waves from local earthquakes are assumed to be composed of single and isotropically scattered body waves over the model space $V$ with a scattering coefficient $g(f, p)$ at the $p$th block. $P_{ij}(f, \tau_{ij}^{\rm obs})$ is then expressed by

$$P_{ij}\left(f, \tau_{ij}^{\rm obs}\right) = \iiint_{\langle p \rangle} \frac{g(f, p)}{r_{ip}^2 r_{pj}^2} \delta V, \quad (5)$$

where $r_{ip}$ and $r_{pj}$ indicate the distances from the centre of the $p$th block to the $i$th earthquake and to the $j$th station, respectively. The summation is done over all the $\langle p \rangle$th block that satisfies the traveltime to be $|\tau_{ij}^{\rm obs} - \tau_{ij}^{\rm cal}(p)| \leq \delta\, t/2$.

We calculate the traveltime $\tau_{ij}^{\rm cal}(p)$ of scattered waves responsible for the observed coda spectrum as the sum of that from the $i$th earthquake to the $p$th block $\tau_{ip}$ plus that from the scatterer to the $j$th station $\tau_{pi}$, including the free surface reflection as an additional contribution from the mirror image source of the $i$th earthquake:

$$\tau_{ij}^{\rm cal}(p) = \tau_{ip} + \tau_{pj}. \quad (6)$$

In order to estimate relative scattering coefficient at each block, $CSF_{ij}(f, \tau_{ij}^{\rm obs})$ defined by eq. (4) as a function of lapse time, $\tau_{ij}^{\rm obs}$, is mapped into the spatial variation of relative scattering coefficient (Fig. 3b). The scattering coefficient $g_{\rm i}j(f, p)$ of the $p$th block in frequency $f$ is estimated from the observed power spectra of coda waves, $CSF_{\rm i}j(f, \tau_{ij}^{\rm obs})$, for a given earthquake–station pair (i.e. $i$th earthquake and $j$th station) by distributing the energy in an isochronal scattering shell with eq. (5) (Fig. 3b):

$$g_{ij}(f, p) = r_{ip}^2 r_{pj}^2 CSF_{ij}\left(f, \tau_{ij}^{\rm obs}\right) \frac{\delta V}{\widetilde{V}\left(\tau_{ij}^{\rm obs}\right)}, \quad (7)$$

where $\widetilde{V}(\tau_{ij}^{\rm obs})$ is the volume of the ellipsoidal shell over the given time interval $(\tau_{ij}^{\rm obs} - \delta t/2, \tau_{ij}^{\rm obs} + \delta t/2)$. We calculate $g_{ij}(f, p)$ for all the earthquake–station pairs (i.e. all the observed combinations of $i$ and $j$) and average them for a given $p$th scatterer (Fig. 4):

$$\widetilde{g}(f, p) = \frac{1}{N \times M} \sum_{i=1}^{N} \sum_{j=1}^{M} g_{ij}(f, p), \quad (8)$$

where $N$ and $M$ are the earthquake and station numbers, respectively. As a result, $\widetilde{g}(f, p)$ represents the relative scattering coefficient in the $p$th block at frequency $f$.

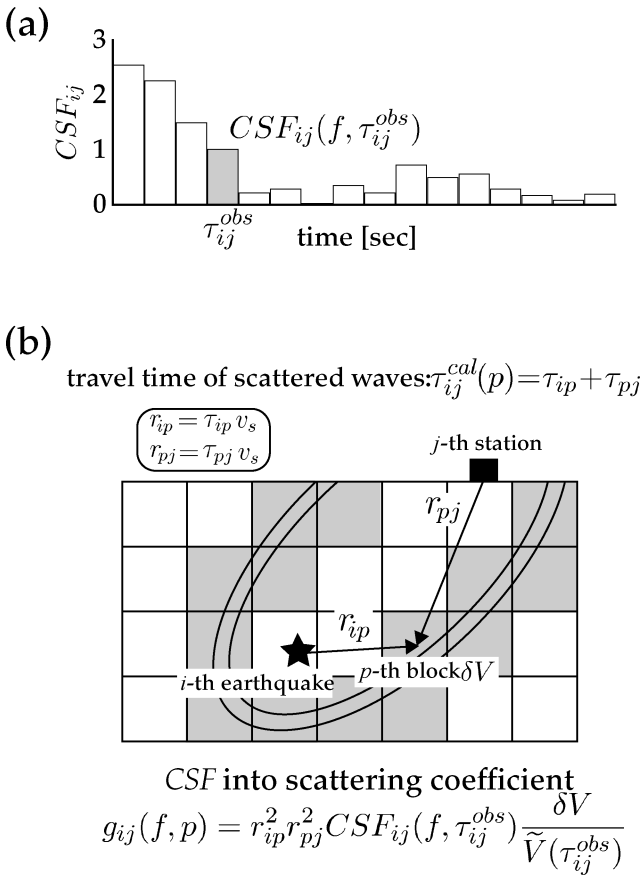


**Figure 3.** Schematic view of dividing $CSF_{ij}(f, \tau_{ij}^{\rm obs})$. (a) One value of $CSF_{ij}(f, \tau_{ij}^{\rm obs})$ for the $i$th earthquake of the $j$th station. (b) Ellipsoidal shell for the given time interval $(\tau_{ij}^{\rm obs} - \delta t/2, \tau_{\rm ij}^{\rm obs} + \delta\, t/2)$. Blocks in grey indicate those imaged from the given $CSF_{ij}(f, \tau_{ij}^{\rm obs})$.

## 3 TECTONIC SETTING AND DATA

The crustal structure in Hokkaido, Japan, is dominated by a series of accretion and collision processes from late Jurassic to the present (e.g. Kimura 1994). There are several active seismic zones around the Hidaka region, a high mountain area in central South Hokkaido, forming two seismic planes (i.e. double seismic zone) in the subducting Pacific Plate (e.g. Hasegawa *et al.* 1978; Suzuki *et al.* 1983; Katsumata *et al.* 2003). In order to estimate its detailed crustal structure, seismic reflection/refraction experiments (e.g. Iwasaki *et al.* 1998; Moriya *et al.* 1998; Tsumura *et al.* 1999) and magnetotelluric (MT) surveys (e.g. Ogawa *et al.* 1994; Uyeshima *et al.* 2001) have been conducted. 3-D seismic tomography studies have been also conducted in this area (e.g. Zhao & Hasegawa 1993; Miyamachi *et al.* 1994; Murai *et al.* 2003). Moriya *et al.* (1998) estimated the *P*-wave velocity structure of the upper crust in this area, using seismic reflection/refraction exploration technique. They suggested that the continental crust of the Kurile Outer Arc overthrusts that of the Northern Honshu Outer Arc as a result of their collisional movement. Taira & Yomogida (2003) obtained the 2-D spatial variation of high-frequency coda amplitude levels in this region. They concluded that strong heterogeneities with the scale of 0.6–1.3 km should be located in the west of the Hidaka Mountains although their locations and magnitudes were not fully constrained.

We applied the imaging method explained in Section 2 to the seismograms recorded by a dense seismic network in this area

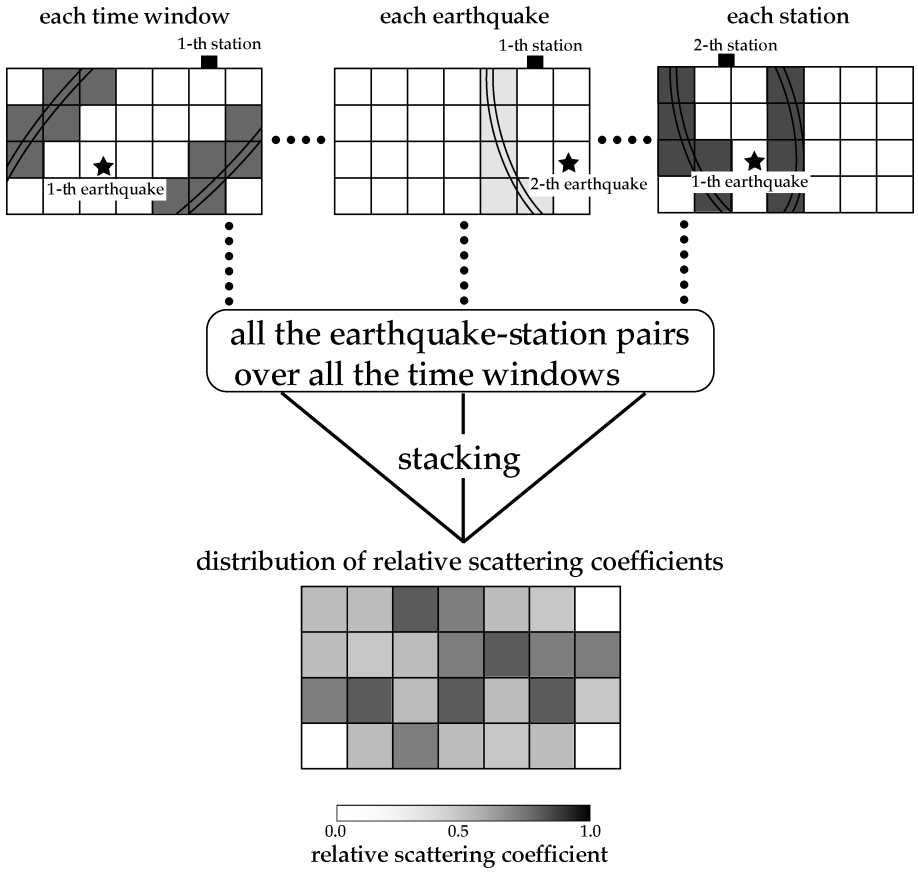


**Figure 4.** Schematic view of obtaining relative scattering coefficients.

operated by the Research Group of Hidaka Collision Zone and the Institute of Seismology and Volcanology, Hokkaido University (e.g. Katsumata *et al.* 2003). Most of the stations were equipped with a three-component 1 Hz velocity seismometer. The sampling rate of all the seismograms was 100 Hz. We used hypocentral parameters determined by Katsumata *et al.* (2003). We selected seven local earthquakes of magnitude greater than 5, in order to obtain seismograms to be analysed under the following criteria: (i) high signal-to-noise ratio and (ii) recorded at most of the stations for a given earthquake. In addition, our data set includes seismograms for the additional two earthquakes used by Taira & Yomogida (2003), in order to compare their 2-D spatial variation of coda levels. Fig. 5 shows 62 stations and epicentres of nine earthquakes used in this study. We analysed seismograms in six frequency bands: 1, 2, 4, 8, 16 and 32 Hz. We used a coda part with a lapse time greater than twice the *S*-wave traveltime. The total time window of 20.48 s is considered for scattered waves to be mapped in our model space (Fig. 2a).

The extent of the model space is shown by the solid square in Fig. 5: 140 × 140 km in horizontals and 150 km in depth. The size of each block $\delta V$ is 20 × 20 km in horizontals and 15 km in depth. We calculated the running power spectrum with a time window ($\delta t$) of 1.28 s (Fig. 2c). In order to determinate such a running power spectrum accurately even in a short-time window, we applied an autoregressive (AR) modelling method (e.g. Akaike 1969; Kanasewich 1973). *S*-wave velocity was set to be 4.0 km s $^{-1}$. This value is nearly equal to the average *S*-wave velocity down to 100 km in this area (Suzuki *et al.* 1988). Because most hypocentres are located within the area covered by our seismic array (Fig. 5), all the ray paths in this study are not far from straight, so that the introduction of any realistic velocity structure will not alter the resulting location of heterogeneities significantly.

To evaluate the spatial resolution of the above approach applied to the present data set, we conducted a so-called checkerboard test. Large ($\widetilde{g} = 0.1$) and small ($\widetilde{g} = 0.01$) relative scattering coefficients are assigned to blocks that are arranged alternately in the model space. We synthesized coda envelopes for the nine analysed earthquakes, using the same modelling procedure, as explained in Section 2. The synthetic data were added Gaussian white noise of 20 per cent of the average signal level. Figs 6 and 7 show the result of this resolution test in horizontal and vertical cross-sections, respectively. We normalized relative scattering coefficients $\widetilde{g}(f, p)$ of eq. (8) by the logarithmic average value. The resolution is high in the central part of the model space. It is especially good 0–90 km deep, except for near edges of the model space. Near edges and the part deeper than 120 km, however, the assigned pattern is not correctly reconstructed.

Fig. 8 shows the histogram of retrieved relative scattering coefficients. Although we set scattering coefficients with high contrast into each block (i.e. 0.1 and 0.01), retrieved scattering coefficients are only slightly different between maximum and minimum values. Relative scattering coefficients with the actual data set in this study covered larger and/or smaller than log average by 0.3, much larger than the test with synthetic data (Fig. 8). Because theses large (and small) values are the result of artificial anomalies with poor resolution created by our imaging process, we removed blocks of such a large (and small) scattering coefficient in our mapping heterogeneities, as shown in the next section.

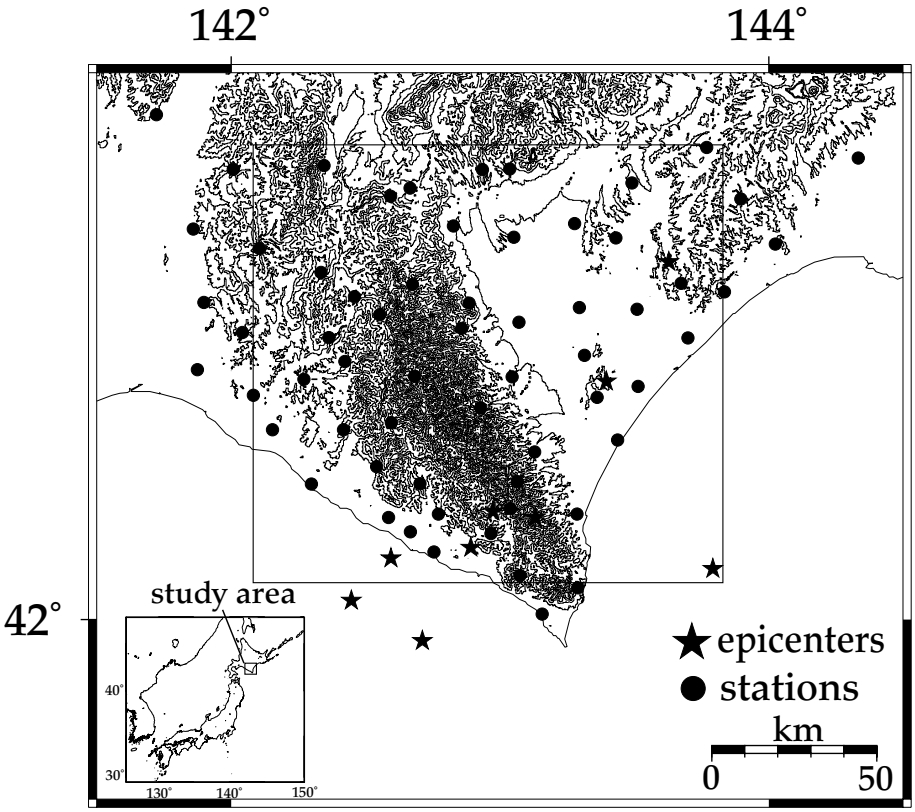


**Figure 5.** Distribution of epicentres (stars) and stations (circles). The model space for imaging heterogeneities is indicated by the solid square. Topographic contour interval is 200 m.

## 4 THREE-DIMENSIONAL DISTRIBUTION OF HETEROGENEITIES IN THE HIDAKA REGION

If the size of heterogeneities is much smaller than the wavelength of the incident wave, the amplitude of scattered waves decreases rapidly, as frequency decreases, for example, the power spectrum decreases as $f^{-4}$, where $f$ is the frequency of scattered wave, which is called Rayleigh scattering. On the other hand, if the size is larger than the wavelength, the amplitude of scattered waves changes weakly with frequency although their azimuthal dependency becomes strong (e.g. Sato & Fehler 1998). These consequences make the observed scattered waves most sensitive to heterogeneities with a size comparable to the wavelength corresponding to the dominant frequency considered. To study the spatial distribution of relative scattering coefficient in terms of scatterers of different sizes, it is important to pay our attention to its frequency dependence.

Using the procedures and the data explained in the previous sections, we obtained $\widetilde{g}(f, p)$, that is, the 3-D distribution of relative scattering coefficient in the Hidaka region. Fig. 9 shows horizontal distributions at 2, 4 and 16 Hz at a depth shallower than 45 km. The most remarkable feature in the obtained distributions of scattering coefficient is a zone of large scattering coefficient in the southwest of the Hidaka Mountains at 2 and 16 Hz. This zone is consistent with the result of Taira & Yomogida (2003), as an area of large coda amplitude factor (*CAF*). On the other hand, the distribution at 4 Hz does not show such specific anomalies, which also agrees with the result of relatively uniform *CAF* distributions at 4 Hz, compared with those at 2 and 16 Hz (Taira & Yomogida 2003). In other words, this located heterogeneous zone can scatter less seismic waves in the intermediate frequency range (4 Hz).

Yomogida *et al.* (1997) computed synthetic scattered waves from several distributions of seismic scatterers, using the boundary integral method. They found that a localized zone of many scatterers generates two spectral peaks of scattered waves. They concluded that the spectral peak in a low-frequency range is originated from the entire zone of scatterers while a high-frequency peak is generated by individual scatterers. The observed coda waves in the southwest of the Hidaka region (Fig. 9) may imply such a localized zone composed of many small heterogeneities, in analogy to Yomogida *et al.* (1997). In addition, the present location of large relative scattering coefficient agrees very well with the clear clustering of microearthquakes that extends down to the depth 0–45 km. This suggests that the distribution of these shallow heterogeneities shows the overall correlation with the seismic activity in this region, as shown in Figs 9(a) and (c). Fig. 10 shows N–S vertical sections of $\widetilde{g}(f, p)$ across the Hidaka Mountains in three frequencies ranges. We focus our attention to three areas of large relative scattering coefficients, as represented in Fig. 10(a), in order to discuss their relationship with the tectonics in this region, for example, the subducting Pacific Plate. Area 1 indicates the upper interface of the subducting Pacific Plate or the upper plane of the double seismic zone, while area 2 corresponds to an intraplate section or the lower plane of the double seismic zone, as determined by the hypocentral distribution shown in Fig. 10 (Katsumata *et al.* 2003). Large scattering coefficients in area 1 are observed only at 16 Hz (Fig. 10c), while scattering coefficients at 2 and 4 Hz are large in area 2 (Figs 10a and b).

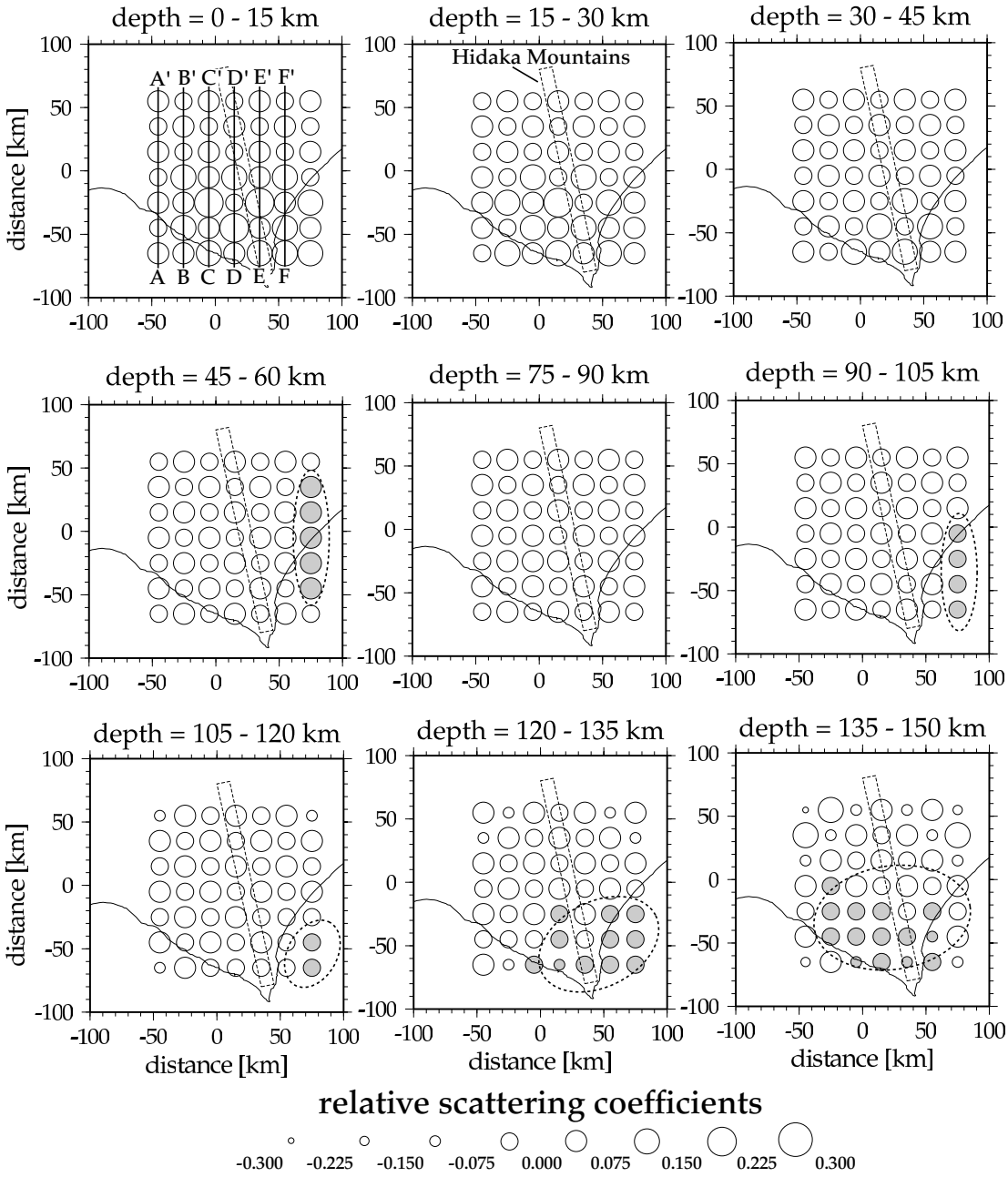


**Figure 6.** Result of a checkerboard test for horizontal sections. The depth range is shown in above each map. Areas of poor resolution are shown by dashed ellipses. Circles in grey indicate those removed from our final result with the data. The magnitude of each relative scattering coefficient is shown by the circle size, as shown along the bottom of the figure.

This clear frequency dependence suggests the existence of two kinds of heterogeneities with different sizes around the subducting Pacific Plate. The characteristic sizes of heterogeneities in areas 1 and 2 are estimated to be approximately 0.08 and 0.32 km respectively (i.e., the corresponding wavelengths of 16 and 4 Hz), assuming the strongest frequency range of scattering to be $kd \simeq 2$ (Yomogida *et al.* 1997), where $k$ is the wavenumber and $d$ is the size of heterogeneities. The large zone of relative scattering coefficient inclines roughly northwards in both areas 1 and 2. These results may be explained by the existence of a strong seismic reflector along the subducting Pacific Plate rather than many point-like scatterers. The distribution of coda level anomalies estimated by Taira & Yomogida (2003) at high frequencies also supports such reflector-type heterogeneities in area 1.

Several studied have detected reflected/scattered waves by a subducting plate. Obara (1997) simulated *S*-coda envelopes, in order to explain the anomalous envelope observed in the Kanto area, using a hybrid model with reflectors and scatterers. He suggested that *S*-coda envelopes are composed of reflected waves from the upper boundary of the subducting Pacific Plate and scattered waves by a two-layered random medium.

On the other hand, there appear to exist relative large scattering coefficients at all frequency ranges in area 3, deeper than 50 km in the southwest of the Hidaka Mountains. However, it is difficult to

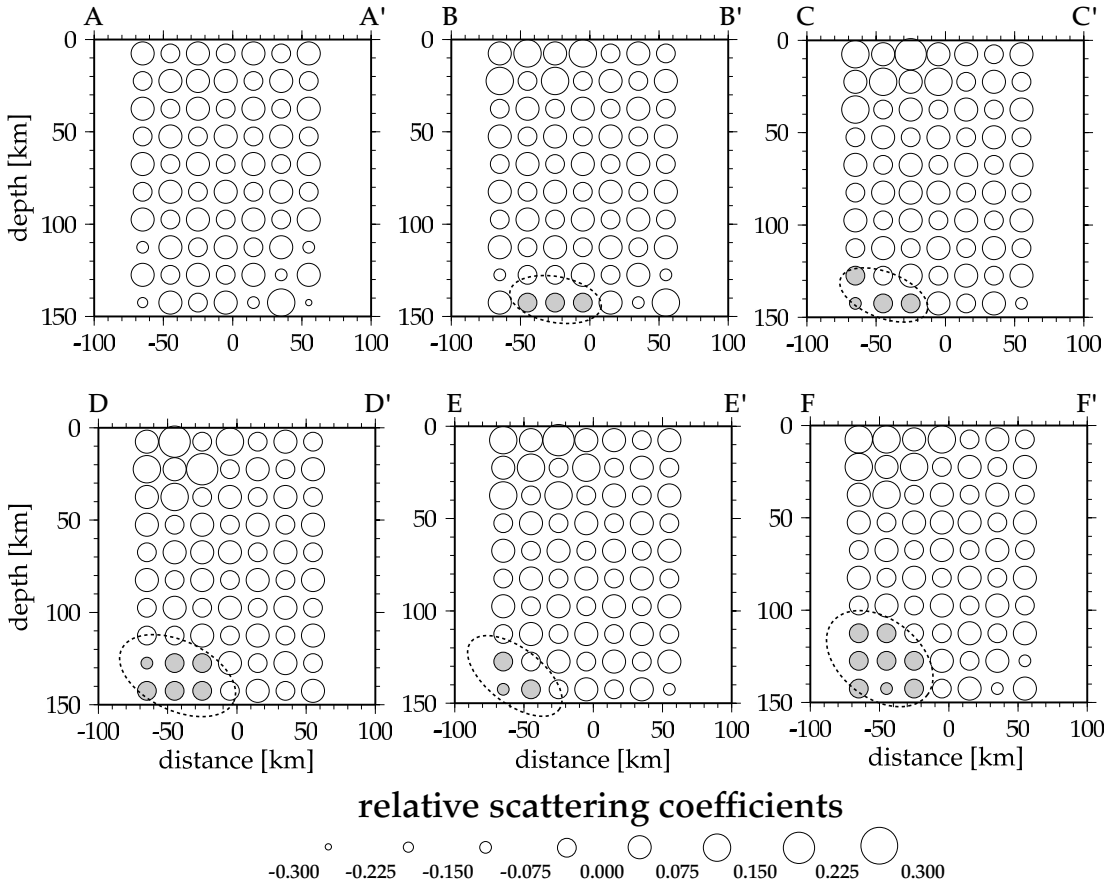


**Figure 7.** Same as Fig. 6 except for vertical cross-sections.

discuss this feature because of the lack of the other geophysical and geological information on the physical properties in this area. As depth increases, relative scattering coefficients become larger in all frequency ranges, probably as a result of the poor resolution there (Fig. 7) and the overestimated effect of $Q_c^{-1}(f)$. Note that we used average $Q_c^{-1}(f)$ for the correction of the overall propagation effect in our model space, as estimated by Taira & Yomogida (2003). Scattering coefficient therefore has large error if $Q_c^{-1}$ has significant and systematic variations in depth and lateral directions and the corresponding ray path is very long. The large relative scattering coefficients in area 3 may be artefacts because of the overestimated effect of $Q_c^{-1}(f)$ and depth (or lateral) dependence in coda $Q$, discussed above. Although it is extremely difficult to correct detail variations of $Q_c^{-1}(f)$, we are currently developing a method to remove the first-order complic of this effect in actual records as the next step of the present study.

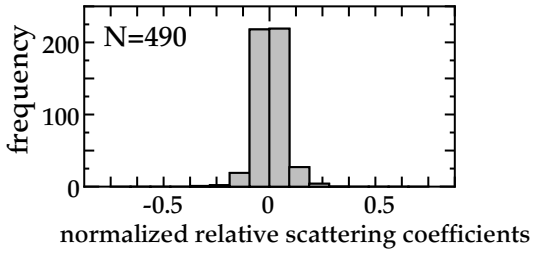


**Figure 8.** Histogram of normalized relative scattering coefficients for the checkerboard test of Figs 6 and 7.

## 5 CONCLUSIONS

We investigated the 3-D distribution of coda scatterers in the Hidaka region from spatial and temporal variations of coda spectra recorded by a dense seismic array. We analysed three-component seismograms in a frequency range from 1 to 32 Hz. After the correction of source, station and over all propagation effects, coda levels were significantly varied, strongly suggesting non-uniform distribution of heterogeneities in this region. In order to pinpoint the locations of heterogeneities, power spectra of coda waves as a function of lapse time were mapped into spatial variations of scattering coefficient, under the following assumptions: spherical radiation from seismic sources, single and isotropic scattering, constant *S*-wave velocity and only *S*-to-*S*–wave conversion.

We revealed the following remarkably non-uniform characteristics in the distribution of relative scattering coefficient in the Hidaka region.

(i) Scattering coefficients at shallow depth (0–45 km) are large in the southwest of the Hidaka Mountains at both 2 and 16 Hz, while any specific pattern anomalies do not appear at 4 Hz. This area corresponds to an area of high microearthquake seismicity, our result suggests several concentrations of many small heterogeneities or probably fractures.

(ii) A clustering of scatterers dipping to the north is located in the two depth ranges, 60–80 (area 1) and 100–120 km (area 2), beneath the Hidaka Mountains. Areas 1 and 2 are composed of

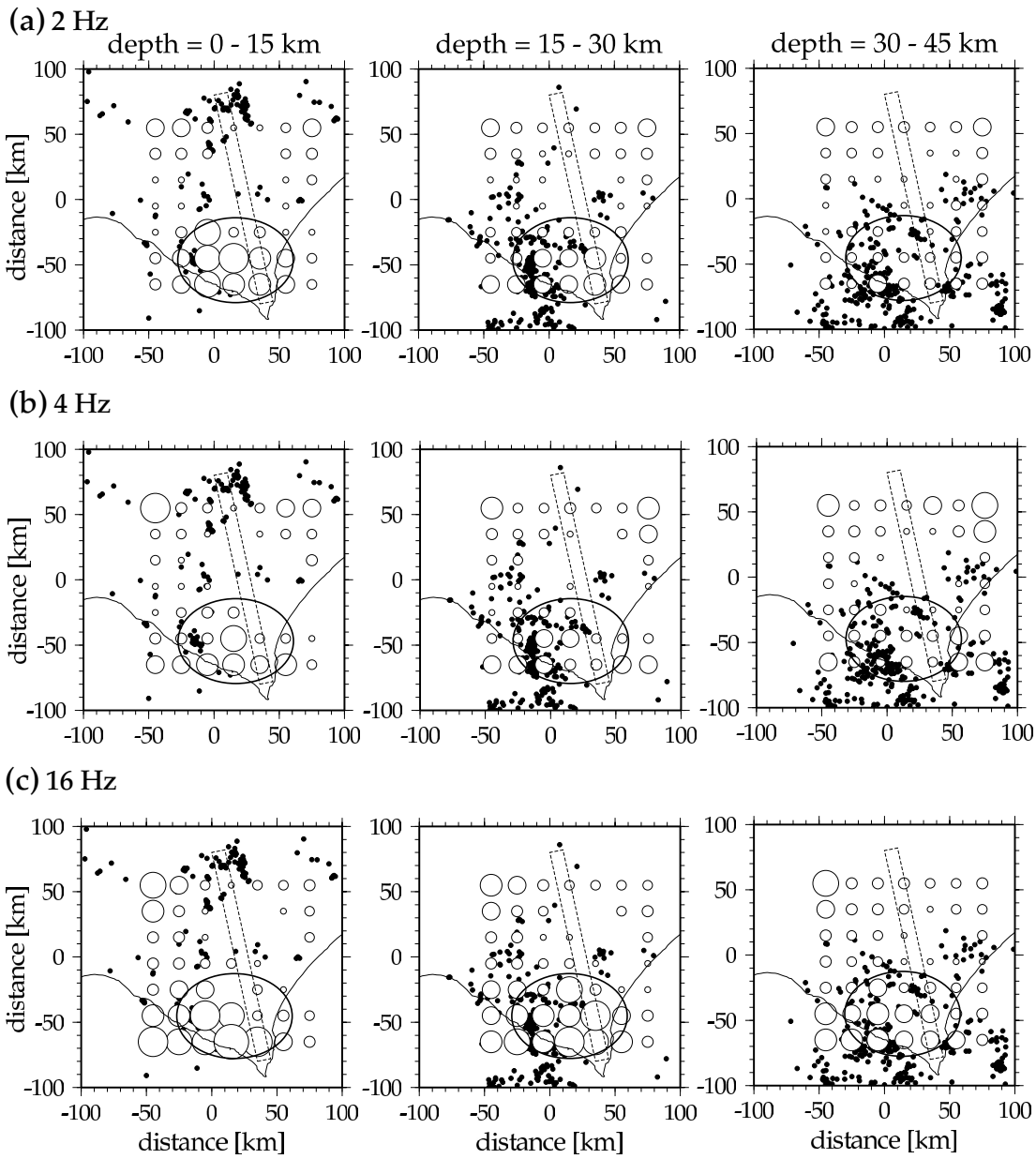


**Figure 9.** Horizontal distributions of relative scattering coefficient for three depth ranges, 0–15, 15–30 and 30–45 km, at (a) 2, (b) 4 and (c) 16 Hz. Areas of large relative scattering coefficient are shown by solid ellipses. Dots indicate the hypocentres in each depth range (modified after Katsumata *et al.* 2003).

heterogeneities with a size of 0.08 and 0.32 km, respectively, from their dominant frequencies. In addition, such zones of strong scattering appear to correspond to heterogeneous zones with the upper and lower planes of the double seismic zone in the subducting Pacific Plate, respectively.

There are several previous studies to interpret an area of strong scattering as a distinguished seismic reflector. Nishigami (1997) estimated the distribution of scatterers around Mt Ontaka, an active volcano in Japan, by the recursive stochastic inversion analysis. He concluded the obtained image of strong scatterers to be a kind of reflective structure. He also found that this image shared a common location and dip with the seismic reflector estimated by the Normal Move-Out (NMO) correction analysis (Inamori *et al.* 1992).

Although we have adopted only the single isotropic model in this study, the above characteristics of the distribution of scatterers are consistent with the distribution of heterogeneities as anomalous features of coda amplification factor formerly estimated by Taira & Yomogida (2003). We can utilize our scattering images in elucidating deep small-scale heterogeneous structures of the Hidaka region. This study employed several assumptions on the scattering process, seismic source radiation and velocity structure. Future studies including more complex phenomena, such as non-isotropic scattering and multiple scattering, will provide clear physical insight into these small-scale heterogeneities in this region. Additional kinds of data, such as polarization and semblance, should also enhance the resolving power of the distribution of heterogeneities.

## ACKNOWLEDGMENTS

The authors thank Dr Kei Katsumata at Hokkaido University for his help in processing of seismic records and providing us with

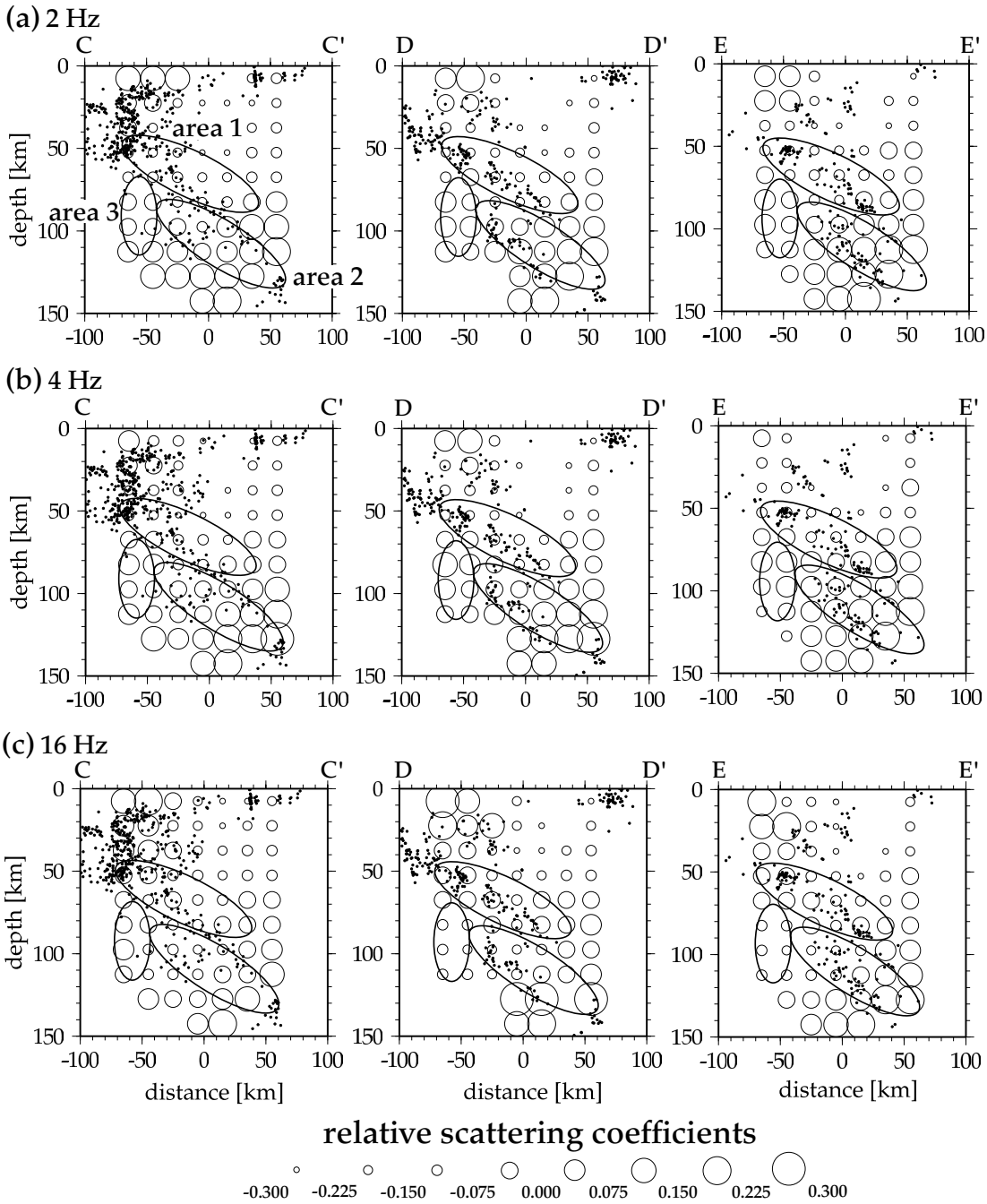


**Figure 10.** Vertical distributions of relative scattering coefficient along the profiles of C–C′, D–D′ and E–E′ in Fig. 6 at (a) 2, (b) 4 and (c) 16 Hz. Three areas of relative scattering coefficients are shown by solid ellipses. Dots indicate the hypocentres in each section (modified after Katsumata *et al.* 2003).

hypocentral parameters used in this paper. The authors also wish to thank Dr Kazunori Yoshizawa at Hokkaido University for constructive comments. Valuable comments by Dr John A. Goff at the Institute for Geophysics, University of Texas, an anonymous reviewer and the editor-in-charge (Dr M. Sambridge) are greatly appreciated. The authors are grateful to the Research Group of Hidaka Collision Zone for their permission for us to use seismic waveform data and to the members of its analysing committee for pre-processing the data. The corresponding observation was conducted by Hokkaido University, Tohoku University, the Earthquake Research Institute, University of Tokyo, Nagoya University, Disaster Prevention Research Institute Kyoto University and Kyushu University, as a part of the new Program of the Study and Observation for Earthquake Prediction. A software package, Generic Mapping Tools (GMT), was used to plot the figures (Wessel & Smith 1995). The present study was partially supported by the Earthquake Research Institute Cooperative Research Program (2000-B-07 and 2001-B-02).

## REFERENCES

Akaike, H., 1969. Fitting autoregressive models for prediction, *Ann. Inst. Statist. Math.,* **21,** 243–247.

Aki, K., 1969. Analysis of seismic coda of local earthquakes as scattered waves, *J. Geophys. Res.,* **74,** 615–631.

Aki, K., 1973. Scattering of *P* wave under the Montana Lasa, *J. geophys. Res.,* **78,** 1334–1346.

Aki, K. & Chouet, B., 1975. Origin of coda waves: Source, attenuation and scattering effects, *J. geophys. Res.,* **80,** 3322–3342.

Aki, K. & Ferrazzini, V., 2000. Seismic monitoring of an active volcano for prediction, *J. geophys. Res.,* **105,** 16 617–16 640.

Capon J., 1969. High-resolution frequency-wavenumber spectrum analysis, *Proc. IEEE,* **57,** 1408–1418.

Gupta, I.N., Lynnes, C.S. & Wagner R.A., 1990. Broadband *F-K* analysis of array data to identify sources of local scattering, *Geophys. Res. Lett.,* **17,** 183–186.

Hasegawa, A., Umino, N. & Takagi, A., 1978. Double-planed structure of the deep seismic zone in the Northern Japan Arc, *Tectonophysics,* **47,** 43–58.

Inamori, T., Horiuchi, S. & Hasegawa, A., 1992. Location of mid-crustal reflectors by a reflection method using aftershock waveform data in the focal area of the 1984 Western Nagano Prefecture earthquake, *J. Phys. Earth,* **40,** 379–393.

Iwasaki, T., Ozel, O., Moriya, T., Sakai, S., Suzuki, S., Aoki, G., Maeda, T. & Iidaka, T., 1998. Lateral structure variation across a collision zone in central Hokkaido, Japan, as revealed by wide-angle seismic experiments, *Geophys. J. Int.,* **132,** 435–457.

Jin, A. & Aki, K., 1986. Temporal change in coda *Q* before the Tangshan earthquake of 1976 and the Haicheng earthquake of 1975, *J. geophys. Res.,* **91,** 665–673.

Kanasewich, E.R., 1973. *Time Sequence Analysis in Geophysics*, The University of Alberta Press, Edmonton, AB, Canada.

Katsumata, K., Wada, N. & Kasahara, M., 2003. Newly imaged shape of the deep seismic zone within the subducting Pacific plate beneath the Hokkaido corner, Japan-Kurile arc-arc junction, *J. geophys. Res.,* **108(B12),** 2565, doi:10.1029/2002JB002175.

Kimura, G., 1994. The latest Cretaceous-early Paleogene rapid growth of accretionary complex and exhumation of high pressure series metamorphic rocks in northwestern Pacific margin, *J. geophys. Res.,* **99,** 22 147–22 164.

Matsumoto, S., Obara, K. & Hasegawa, A., 1998. Imaging *P*-wave scatterer distribution in the focal area of the 1995 M7.2 Hyogo-ken Nanbu (Kobe) Earthquakes, *Geophys. Res. Lett.,* **25,** 1439–1442.

Miyamachi, H., Kasahara, M., Suzuki, S., Tanaka, K. & Hasegawa, A., 1994. Seismic velocity structure in the crust and upper mantle beneath northern Japan, *J. Phys. Earth,* **42,** 269–301.

Moriya, T., Okada, H., Matsushima, T., Asano, S., Yoshii, T. & Ikami, A., 1998. Collision structure in the upper crust beneath the Southwestern foot of the Hidaka Mountains, Hokkaido, Japan as derived from explosion seismic observations, *Tectonophysics,* **290,** 181–196.

Murai, Y. *et al.,* 2003. Delamination structures imaged in the source area of the 1982 Urakawa-oki earthquake, *Geophys. Res. Lett.,* **30(9)**, 1490, doi:10.1029/2002GL016459.

Neidell, N.S. & Taner, M.T., 1971. Semblance and other coherency measures for multichannel data, *Geophysics,* **36,** 482–497.

Nikolaev, A.V. & Troitskiy, P.A., 1987. Lithospheric studies based on array analysis of P-coda and microseisms, *Tectonophysics,* **140,** 103–113.

Nishigami, K., 1991. A new inversion method of coda waveforms to determine spatial distribution of coda scatterers in the crust and uppermost mantle, *Geophys. Res. Lett.,* **18,** 2225–2228.

Nishigami, K., 1997. Spatial distribution of coda scatterers in the crust around two active volcanoes and one active fault system in central Japan: Inversion analysis of coda envelope, *Phys. Earth planet. Int.,* **104,** 75–89.

Nishigami, K., 2000. Deep crustal heterogeneity along and around the San Andreas fault system in central California and its relation to the segmentation, *J. geophys. Res.,* **105,** 7983–7998.

Obara, K., 1997. Simulations of anomalous seismogram envelopes at coda positions, *Phys. Earth planet. Int.,* **104,** 109–125.

Ogawa, Y., Nishida, Y. & Makino, M., 1994. A collision boundary imaged by magnetotellurics, Hidaka Mountains, Central Hokkaido, Japan, *J. geophys. Res.,* **99,** 22 373–22 388.

Revenaugh, J., 1995. A scattered-wave image of subduction beneath the Transverse Ranges, *Science,* **268,** 1888–1892.

Revenaugh, J., 2000. The relation of crustal scattering to seismicity in southern California, *J. geophys. Res.,* **105,** 25 403–25 422.

Sato, H. & Fehler, M.C., 1998. *Seismic Wave Propagation and Scattering in the Heterogeneous Earth*, Springer-Verlag, New York.

Sato, H., Nakahara, H. & Ohtake, M., 1997. Synthesis of scattered energy density for non-spherical radiation from a point shear dislocation source based on the radiative transfer theory, *Phys. Earth planet. Int.,* **104,** 1–13.

Su, F. & Aki, K., 1990. Temporal and spatial variation of coda $Q^{-1}$ associated with the North Palm Springs earthquake of July 8, 1986, *Pure appl. Geophys.,* **133,** 23–52.

Suzuki, S., Sasatani, T. & Motoya, Y., 1983. Double seismic zone beneath the middle of Hokkaido, Japan, in the southwestern side of the Kurile Arc, *Tectonophysics,* **96,** 59–76.

Suzuki, S., Takanami, T., Motoya, Y. & Nakanishi, I., 1988. A real-time automatic processing system of seismic waves for the network of Hokkaido University, *J. seism. Soc. Japan, Ser. 2,* **41,** 359–373 (in Japanese with English abstract).

Taira, T. & Yomogida, K., 2003. Characteristics of small-scale heterogeneities in the Hidaka, Japan, region estimated by coda envelope level, *Bull. seism. Soc. Am.,* **93,** 1531–1541.

Tsumura, N. *et al.*, 1999. Delamination-wedge structure beneath the Hidaka Collision Zone, Central Hokkaido, Japan inferred from seismic reflection profiling, *Geophys. Res. Lett.,* **26,** 1057–1060.

Tsuruga, K., Yomogida, K., Ito, H. & Nishigami, K., 2003. Detection of localized small-scale heterogeneities in the Hanshin-Awaji region, Japan, by anomalous amplification of coda level, *Bull. seism. Soc. Am.,* **93,** 1516–1530.

Uyeshima, M., Utada, H. & Nishida, Y., 2001. Network-magnetotelluric method and its first results in central and eastern Hokkaido, NE Japan, *Geophys. J. Int.,* **146,** 1–19.

Wessel, P. & Smith, W.H.F., 1995. New version of the Generic Mapping Tools released, *EOS, Trans. Am. Geophys. Un.,* **76,** 329.

Yomogida, K., Benites, R., Roberts, P.M. & Fehler, M., 1997. Scattering of elastic waves in 2-D composite media II. Waveforms and spectra, *Phys. Earth planet. Int.,* **104,** 175–192.

Zhao, D. & Hasegawa, A., 1993. *P* wave tomographic imaging of the crust and upper mantle beneath the Japan Islands, *J. geophys. Res.,* **98,** 4333–4353.